Supplementary Figures

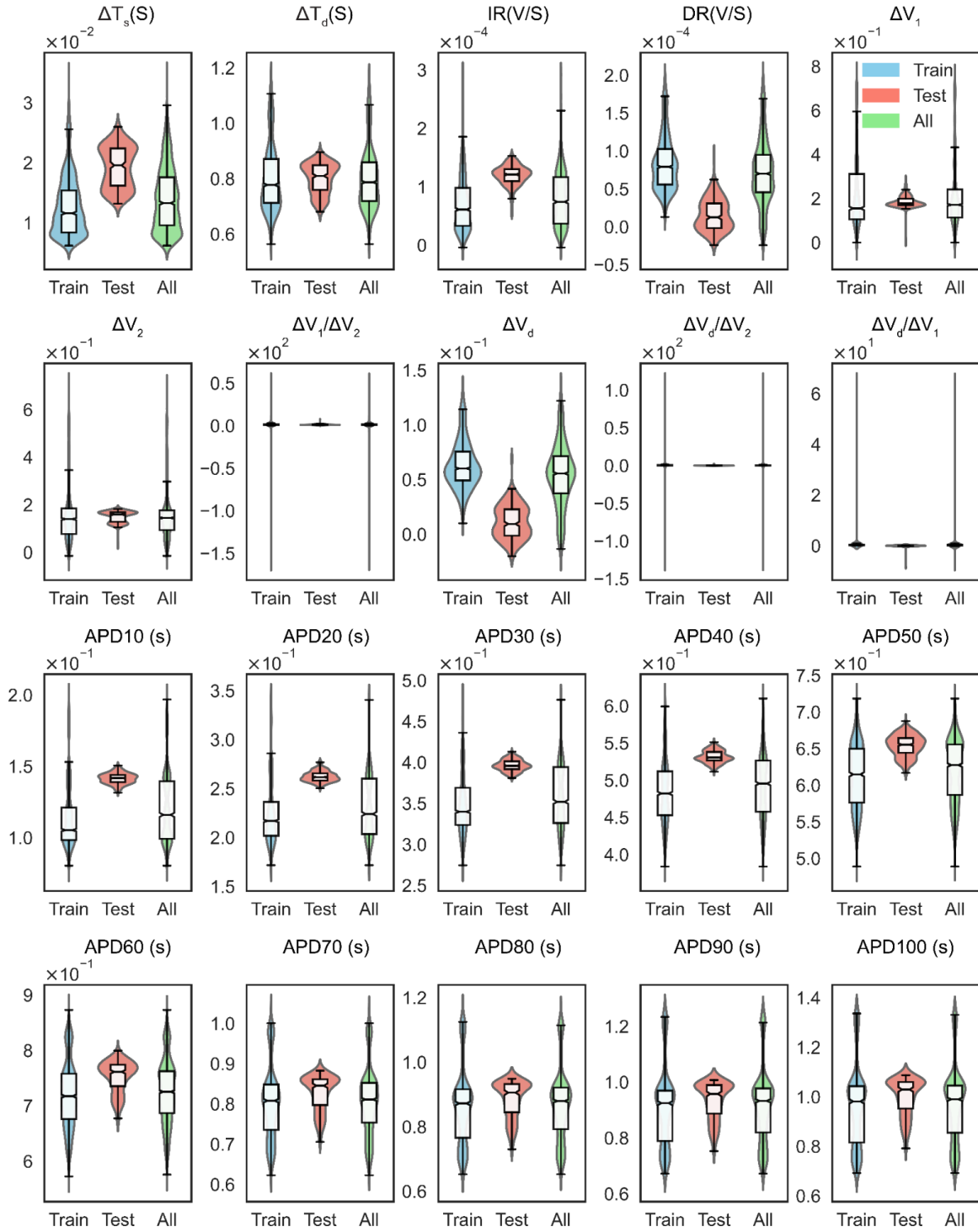## Distribution of eAP and iAP Features

Figure SF-1. a) Violin plot distribution of eAP and iAP features for the data utilized in the machine learning and deep learning models, as depicted in Figure-3b, shown in green. The blue and red plots represent the distribution of the training set and test set for eAP and iAP, respectively.
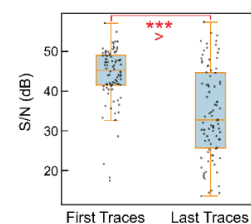
a iAPs APD Changes with Stepwise Dofetilide Doses (0.3,1,3, and 10 nM) During Recording Sessions
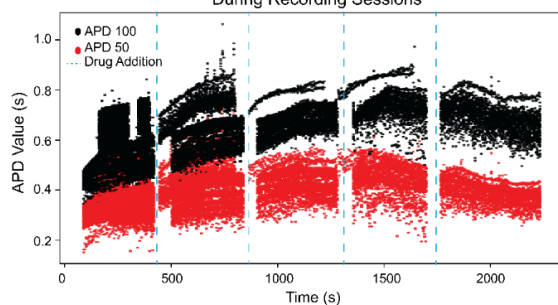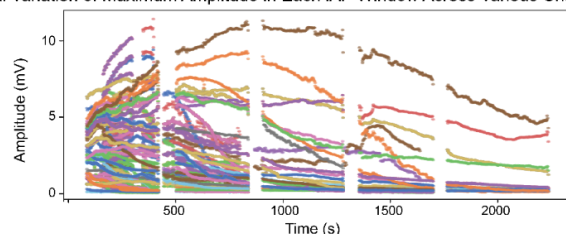
b Temporal Variation of S/N Each iAP Window Across Different Channel Recordings
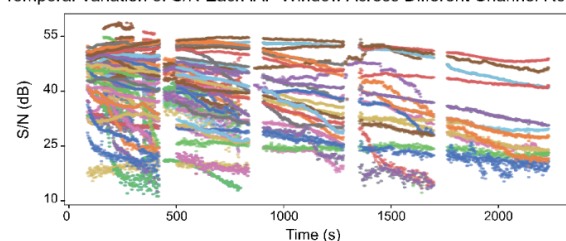
c iAP First Vs Last Traces S/N

d Temporal Variation of Maximum Amplitude in Each iAP Window Across Various Channel Recordings
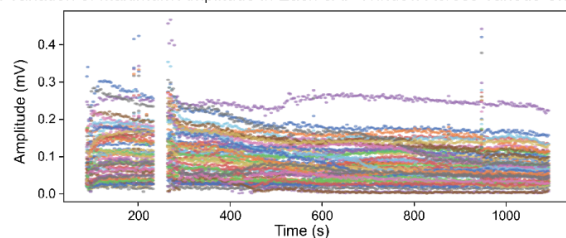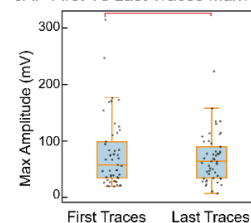
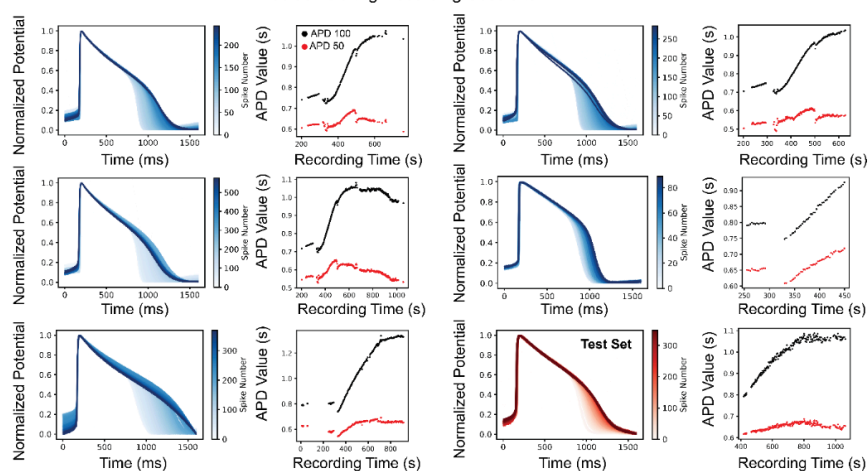**e** iAP First Vs Last Traces Max Amplitude
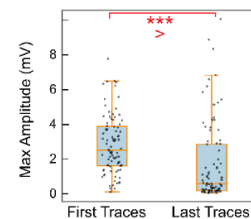
f Temporal Variation of Maximum Amplitude in Each eAP Window Across Various Channel Recordings

g eAP First Vs Last Traces Max Amplitude

h iAPS Change and iAPs APD Response to Single Step10 nM Dofetilide Addition During Recording Sessions

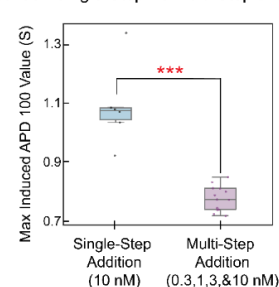**i** Comparing Max Induced APD 100 between Single-Step Vs Multi-Step Drug addition

Figure SF-2. a) Comparison of iAP APD values upon drug addition, based on experiments comparing neighboring NEA channels' iAPs, from 88 unique iAP channels across two sets of recordings. The dashed line indicates the time of drug addition. **b)** Showcase of the variation in iAP signal-to-noise ratio (S/N) over time from the same recordings as above. **c)** Comparison of the last iAP in the recording with the first one in terms of S/N, demonstrating a significant drop in value (P value = [***p-value: 8.63 x 10^{-15}]) as the experiment progresses, due to the resealing of cell membrane pores. **d)** Presentation of the variation in iAP window's maximum amplitudes (spike amplitude) over time from the same recordings as above. **e)** Comparison of the last iAP in the recording with the first one in terms of amplitude, showing a significant drop in value (***p- value = [1.1 x 10^{-08}]) as the experiment progresses, attributed to the resealing of cell membrane pores. **f)** Presentation of the variation in eAP maximum amplitude (spike amplitude) over time for 49 distinct eAP channels. **g)** Comparison of the last eAP in the recordings with the first one in terms of amplitude, indicating no significant change (p- value = [0.262]). **h)**iAPs collected from distinct sets of recordings by the addition of dofetilide, used for the machine learning and deep learning aspects of this study.
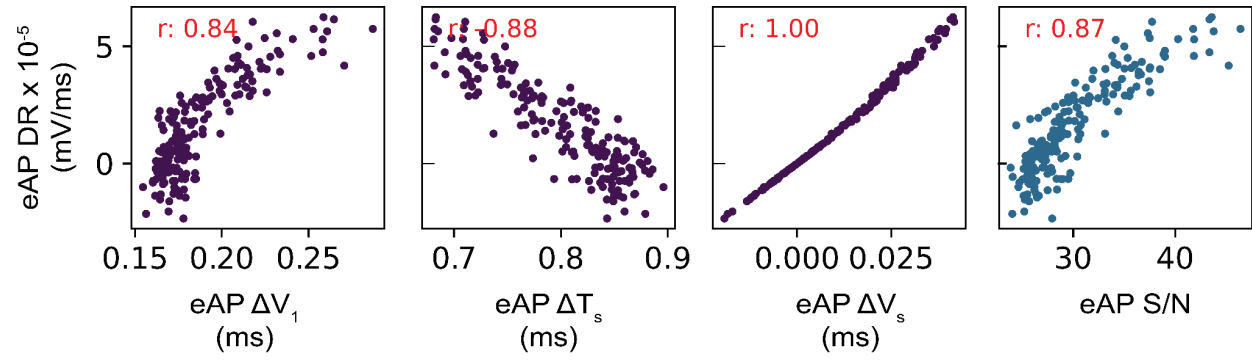
Figure SF-3. Qunatille-Physics-Informed Attention Unet (QPIA-UNET) can reconstruct the entire iAP waveform from the eAP signal with confidence interval. a) QPIA-UNET Model Schematic: This provides a visual representation of the QPIA-UNET model used in the study. The model simultaneously predicts three potentials (V1, V2, V3) represented in green (V1, q = 0.05), red (V2, q = 0.5), and blue (V3, q = 0.095), along with their corresponding physics parameters (k1 and a1 in green, k2 and a2 in red, and k3 and a3 in blue) from the bottleneck. **b)** This illustrates how the model's predicted potential values closely align with actual values, achieving a coefficient of determination (r² = 0.98). **c)** The model demonstrates a MAE of 0.055 ± 0.017 on the test set, compared to a lower MAE of 0.014 ± 0.020 on the training set. **d)** Reconstructed iAPs from the median predictor (q = 0.5) are compared with actual ones in terms of APD, revealing APD errors at 30%, 50%, 70%, and 90% repolarization levels of 0.014 ± 0.012 s, 0.017 ± 0.012 s, 0.033 ± 0.016 s, and 0.074 ± 0.020 s, respectively. These errors correspond to percentage errors of 3.624 ± 2.976%, 2.611 ± 1.806%, 3.957 ± 1.906%, and 7.833 ± 1.904%. **e)** The cumulative absolute error from APD 10 to APD 100 for both test and training samples is presented, with a mean total APD error of 0.331 ± 0.086s for the test set and 0.262 ± 0.756s for the training set.

Figure SF-4. Correlation between eAP features in the test set used to evaluate the XGBoost and deep learning models.